Heliyon 10 (2024) e24191

Contents lists available at ScienceDirect

Heliyon

journal homepage: www.cell.com/heliyon

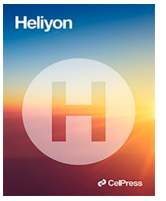

Research article

One-pot synthesis optimization of thiol-capped SnS and SnS/ZnS QDs for photocatalytic degradation of Rhodamine 6G

Madillo Mareka, Mangaka Matoetoe, Ncediwe Tsolekile *

Chemistry Department, Cape Peninsula University of Technology, PO Box 1906, Bellville, 7535, South Africa

ARTICLE INFO

Keywords:
SnS
Thiol capping
SnS/ZnS
Quantum dots
Dye degradation
Rhodamine 6G

ABSTRACT

Interest in SnS-based quantum dots (QDs) has increased due to their low toxicity, widespread natural availability, and superior electro-optical characteristics suitable for photodegradation applications. Herein, we report the synthesis of SnS-based QDs using thiourea and tin (II)chloride as salt precursors. The study explored the impact of various synthetic parameters such as pH, capping ligand, Sn:S ratio, reaction solvent, and ZnS shell on the optical characteristics of the synthesized QDs. The optimal QDs properties were observed at pH = 3 and Sn:S ratio = 1:1. Transmission electron microscopy analysis showed spherical nanoparticles, while the Fourier Transform Infrared spectroscopy revealed QDs with thiol capping. Time-dependent studies revealed that when the QDs were synthesized using propylene glycol, the ultraviolet-visibile (UV–vis) spectrum exhibited an increase in absorbance over time and improved stability compared to aqueous synthesized QDs. SnS/ZnS QDs capped with 3-mercaptopropanoic acid exhibited improved photoluminscence (PL) emissions, stability, and aqueous dispersion compared to glutathione and L-Cysteine as thiol-capping agents. The photocatalytic activity of SnS/ZnS QDs was assessed against Rhodamine 6G and increased to 65 % when passivated with ZnS compared to 31 % for the core SnS QDs. With the given findings, this study supports the stability and effectiveness of the SnS/ZnS QDs as a viable dye degradant.

1. Introduction

Water scarcity is a global challenge, with approximately 20 % of industrial water pollution attributed to textile emissions. The presence of textile dyes, organic micro molecules, and non-biodegradable materials in wastewater poses a public health concern and a global environmental challenge [1,2]. Addressing the removal of these pollutants is essential as access to safe and clean water is recognized as a worldwide priority for long-term economic growth and societal well-being [3]. Various conventional approaches, including biological oxidation, chemical-physical treatment adsorption, sedimentation, and coagulation [2,4], have been employed to remove dyes in wastewater. However, these methods are reported to be inefficient in achieving the desired level of degradation due to the stable large degree of aromatic groups in dye molecules and complex chemical structures [5]. The photocatalytic process has gained considerable attention in wastewater treatments due to its ease of availability, low cost, simplicity, and high efficiency [6]. In this process, metal oxides (e.g., ZnO, TiO_2, Fe_2O_4) [5], ferrates (e.g., $GdFeO_3$, K_2FeO_4) [7], and traditional quantum dots (QDs) (e.g., CdSe, CdTe) [8] have served as low-cost, visible-light-driven photocatalysts with high absorption efficiency. However, metal oxides suffer from charge carrier recombination, undesirable wide-band gaps, and limited visible response [9]. In contrast, the uncontrollable

* Corresponding author.
E-mail address: tsolekilen@cput.ac.za (N. Tsolekile).

https://doi.org/10.1016/j.heliyon.2024.e24191
Received 25 July 2023; Received in revised form 29 December 2023; Accepted 4 January 2024
Available online 5 January 2024

recombination rate of ferrates and the inherent toxicity of Cd-based QDs are undesirable for photocatalysis and disadvantage their industrial use.

SnS-QDs present several advantages over conventional catalysts for the photocatalytic process, including a high absorption coefficient (>104 cm^{-1}), quantum confinement effects, and a narrow and indirect band gap (1.2–1.5 eV) [10]. Moreover, SnS QDs possess inherent properties such as low toxicity, excellent electro-optical properties, and abundant natural material, enabling their application in various fields such as solar cells and batteries [11], biomedical sensing [12], and medical probes [13]. Compared to commercial catalysts, SnS exhibits several advantages, including tunability for optimizing the photocatalytic process, enhanced stability for longevity and effectiveness of the QDs over time, and low-cost visible-light-driven photocatalysis [14]. However, a literature survey has revealed that very few works [15–17] have been reported on applying SnS QDs for the photocatalytic degradation of Rhodamine 6G. Additionally, to the best of our knowledge, there has been no report on (i) the effect of synthetic solvent on the photoluminescence and absorption behavior of SnS-based QDs and (ii) the effect of ZnS coating on degradation efficiency.

This study reports on the one-pot synthesis of SnS QDs using thiourea and sodium sulfide as dual sulphur sources and stabilizing agents. The use of glycol as a solvent in the synthesis process is advantageous, as propylene glycol contributes to both the stability of the QDs and catalyzes the decomposition process, generating additional radicals that enhance the degradation of pollutants [18]. To improve the efficiency of SnS/ZnS QDs and tailor the properties of the QDs for photocatalytic applications, a systematic investigation of the effect of Sn: S ratio (1:1, 1:2, 1:4, 1:6, and 1:8), pH (3, 5, 7, and 9), capping ligands (glutathione, L-cysteine, and mercapto-propanoic acid), and synthesis solvents ($C_3H_8O_2$ and H_2O) was performed. To understand the structural and optical properties of the QDs, optical and structural characterization was carried out using Photoluminescence (PL) spectroscopy, Ultraviolet–visible (UV–vis), Fourier transform infrared spectroscopy (FTIR), X-ray diffraction (XRD), Dynamic Light Scattering (DLS), Energy-dispersive X-ray spectroscopy (EDS), Scanning Electron Microscope (SEM), and Transmission Electron Microscopy (TEM). Due to the high stability and optical properties of the synthesized SnS QDs, the study evaluated the photodegradation efficiency of SnS/ZnS QDs toward Rhodamine 6G (R6G). Herein, the reproducibility of the synthesis method for water-soluble and stable SnS-based QDs serves as a fundamental property for scalability and practical application, addressing a challenge in the field. The synthesized SnS-based QDs exhibited robust concentration-dependent photocatalytic activity towards R6G, with SnS/ZnS QDs exhibiting superior degradation efficiency compared to the core SnS QDs.

2. Experimental section

2.1. Materials

Tin chloride dihydrate ($SnCl_2$–$2H_2O$), sodium hydroxide (NaOH), hydrochloric acid (HCl), propylene glycerol ($C_3H_8O_2$), thiourea (CH_4N_2S), zinc acetate dihydrate ($Zn(ac)_2.2H_2O$), Rhodamine 6G (R6G), L-Cysteine (L-Cys), 3-mercaptopropionic acid (MPA) and glutathione (GSH) were purchased from Sigma–Aldrich, South Africa. All chemicals were of analytical grade and used without further purification.

2.2. Synthesis of thiol-capped SnS QDs

2.2.1. Preparation of stock solutions

The tin stock solution (0.08 M) was prepared by dissolving $Cl_2H_4O_2Sn$ (0.30 g, 1.32 mmol) in 20 ml of $C_3H_8O_2$. The thiourea stock solution (0.08 M) was prepared by dissolving thiourea (0.29 g, 3.8 mmol) in 15 ml of $C_3H_8O_2$, while the L-Cysteine stock solution (0.32 M) was obtained by dissolving L-Cysteine (0.55 g, 4.5 mmol) in 15 ml of $C_3H_8O_2$. MPA stock solution (0.32 M) was prepared by dissolving MPA (0.55 g, 5.18 mmol) into 15 mL of $C_3H_8O_2$, and GSH stock solution (0.32 M) was prepared by dissolving GSH (0.55 g, 1.79 mmol) into 15 mL $C_3H_8O_2$.

ZnS shell precursor: Zn stock solution (0.08 M) was prepared by dissolving 0.3 6 g (Zn (ac) $_2.2H_2O$ in 15 mL propylene glycol. The sulphur stock solution (0.08 M) was prepared by dissolving 0.29 g of thiourea in 15 ml of propylene glycol.

2.2.2. Synthesis of SnS QDs

SnS QDs were synthesized by heating 20 ml of propylene glycerol in an open beaker under magnetic stirring using the modified method by Cheng et al., 2020 [19]. 4 ml thiol capping agent (i.e., GSH, L-Cysteine, and MPA) stock solution was added to the reaction solution. This was followed by the addition of 3 ml of $Cl_2H_4O_2Sn$ stock solution. The pH of the reaction mixture was adjusted to the required pH value. The solution was stirred continuously for 10 min to allow the thiol capping agent to react with Sn while the pH was maintained using NaOH. Then 1 ml of thiourea was added, and the pH of the solution was adjusted using HCl. After the addition of thiourea, the solution turned yellow, and the colour of the solution became intense with an increase in time, confirming the formation of SnS QDs. 4 ml of MPA was added to the synthesis pot to neutralize the positively charged Sn^{2+} followed by 4 ml of the $Cl_2H_4O_2Sn$ stock solution at a constant temperature. The beaker contents were subsequently heated at 70 °C for 60 min to obtain SnS QDs. Different aliquots were taken for every 15 min of the reaction for characterization. The experiment was optimized by varying different synthetic parameters such as the Sn: S ratio (1:1, 1:2, 1:4, 1:6, 1:8), pH (3, 5, 7, and 9), reaction solvent (H_2O vs. $C_3H_8O_2$), thiol capping (GSH, MPA, and L-Cysteine).

2.2.3. Synthesis of SnS/ZnS QDs

Synthesis of SnS/ZnS QDs was synthesized by taking 10 ml of the synthesized SnS-QDs and heating to 70 °C and the pH of the

solution was adjusted to 9 with NaOH. Then 0.08 M of the Zn precursor was added to the solution and mixed for 30 min. Then 0.08 M of the thiourea (sulphur source) was added to the solution and mixed for another 30 min. The solution was precipitated by adding a dilute solution of water and propylene glycol in a 1:1 ratio to the mixture. The entire solution was centrifuged at 6000 rpm for 5 min; the procedure was repeated three times to obtain SnS/ZnS QDs in powder form.

3. Measurement of photocatalytic activity

The photodegradation efficiency of the R6G dye was evaluated under ultraviolet–visible (UV–vis) radiation. A 250W Lelesil photochemical reactor was used as a light source. In a typical photocatalytic process, 2 mg of SnS QDs was added to 100 ml of solution dye. The mixture was stirred and UV irradiated with 250 W at 200–400 nm wavelength at 1000 rpm. ~3.0 ml aliquots were withdrawn from the reaction mixture at fixed time intervals (20 min). The aliquots were analyzed using a UV–vis spectrophotometer to monitor the degradation of R6G over time.

The photodegradation efficiency was calculated using Eq. (1). As follows:

$$\%\ \text{Photodegradation efficiency (PE)} = \left(A_{0-\frac{A}{A_0}} \right) x\ 100 \quad (1)$$

where A_0 = initial absorbance of the dye and.

A = variable absorbance.

4. Characterization

The synthesized SnS and SnS/ZnS QDs were characterized using, Ultraviolet–visible absorption spectrophotometry (UV–vis) (PerkinElmer UV–Vis Lambda 25 spectrometer, UK), Photoluminescence (PL) spectra were collected using a PerkinElmer spectrometer, Fourier Transform infrared spectroscopy (FTIR) was measured using a Spectrum two UATR spectrometer, PerkinElmer, UK. Dynamic Light Scattering (DLS) Malvern P analytical. Transmission electron microscopy (TEM). Powder X-ray diffraction (PXRD) was analyzed using Bruker D8. Advance diffractometer with monochromatic Cu-Kα1 radiation (λ = 1.5418 Å).

5. Results and discussion

5.1. The influence of the Sn:S ratio

The reaction between propylene glycol and thiourea was colourless at ambient temperature; upon introducing of Sn precursor a colour change to orange was observed, indicating the formation of SnS QDs. The precursors (Sn, S, and ZnS) were added in that sequence and at a regulated pH to speed up the reaction between Sn and S. The tunning of the optical properties and elemental control during the synthesis resulted in the formation of pure-phase SnS QDs. Fig. 1 depicts how variations in the Sn: S molar ratios affected the optical (UV–vis and PL) characteristics of SnS QDs. While other stoichiometric ratios showed band-edge absorption, the 1:1 ratio (Sn: S) produced a characteristic broad absorption peak at 234 nm (Fig. 1(a)) consistent with the literature [20]. Herein, the band edge absorption was noted at the curve's most pronounced bend and departure from the longer background wavelength [21].

The corresponding PL (Fig. 1(b)) displayed broad emission peaks in the 350–360 nm region with a maximum emission intensity at 1:1 (Sn:S). The UV–vis region-based emissions suggest the material's potential use in optical devices, while the broad emission is attributed to probable trap states inside the nanocrystals [22,23]. Since Sn:S ratio of 1:1 exhibited the highest intensities, it was subsequently employed throughout the study.

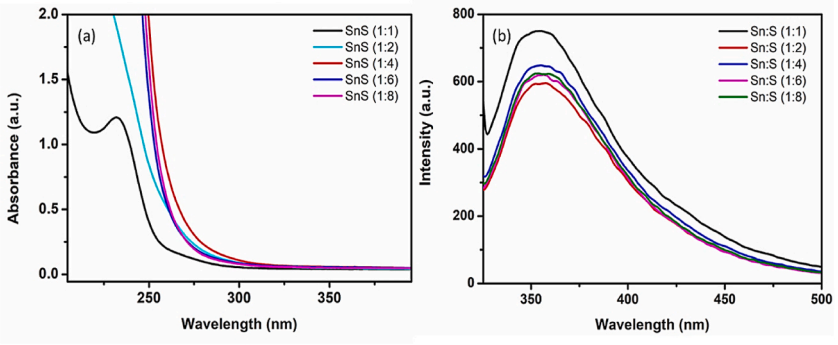

Fig. 1. The effect of the Sn: In ratio on (a) absorbance spectra and (b) photoluminescence of synthesized SnS QDs.

5.2. The influence of pH

pH plays a critical factor in the stability, solubility, and aggregation of QDs. Under neutral and basic conditions, Sn-based QDs are highly soluble, but under neutral conditions, they are unstable [24]. This work assessed the optical characteristics of SnS QDs synthesized in acidic, neutral, and basic solutions. The temporal development of the SnS QDs UV–vis and PL characteristics over various pH levels is depicted in Fig. 2 (a and b). Broad absorbances were observed in the UV–vis, which slightly blue shifted as the pH increased (Fig. 2(a)). Additionally, the absorbance increased with increasing pH, indicating that the particle size decreased under basic conditions. The matching PL at various synthetic pHs is shown in Fig. 2(b). Chen et al. [19], reported on the dissolution of SnS QDs at high pH with little to no emission. Herein, a drop in luminescence intensity was observed as the pH increased. This shows that the surface environment of SnS QDs changes under both acidic and basic conditions. These findings emphasize how pH affects the optical characteristics of Sn-based nanomaterials, similar to those reported in the literature [24,25]. The best pH for this study was selected as pH 3 due to the high PL intensities.

5.3. The influence of synthetic solvent

Synthetic solvents function as soft templates or structure-directing agents that regulate the nucleation and development of QDs to control their size and shape [26]. This work investigated the effect of synthetic solvents on the optical properties of the QDs. The QDs synthesized from propylene glycol and water showed comparable absorption characteristics (Fig. 2(c and d)). A typical decrease in absorption pattern over time was observed when water was utilized as a solvent (Fig. 2(c)). Time-dependent studies revealed that when the QDs were synthesized using propylene glycol, the UV–vis spectrum exhibited an increase in absorbance over time. Conversely, aqueous-synthesized SnS QDs showed a firm settlement after a few days of storage (inset Fig. 2(c)), indicating the instability of SnS QDs in an aqueous environment in line with the literature [19]. Propylene glycol-based SnS QDs remained stable for over 14 days without precipitation (inset Fig. 2(d)). Subsequently, propylene glycol was selected as the synthesis solvent throughout the study.

5.4. The influence of capping ligands

The stabilization and prevention of QDs agglomeration depend heavily on capping agents. Thiol capping agents offer surface tuning through further surface modification, which permits the QDs use in various applications [26]. Thiols also have a strong attraction for metal-based surfaces. In this study, three thiol capping agents; L-cysteine, 3-mercaptopropanoic acid (MPA), and glutathione (GSH),

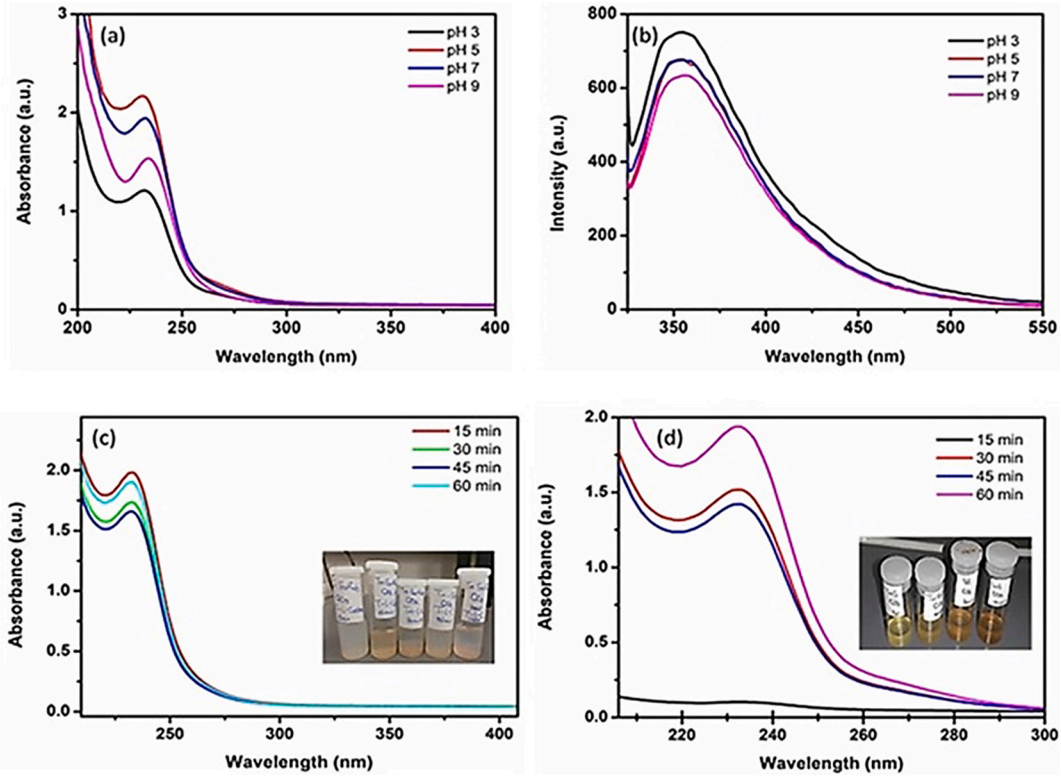

Fig. 2. The effect of pH on (a) absorbance spectra and (b) photoluminescence of synthesized SnS QDs. The effect of synthetic solvent (c) water and (d) propylene glycol on the absorption spectra (insets: digital photograph of SnS QDs synthesized in (c) water and (d) propylene glycol).

were used to assess the impact of the capping agents on the optical properties of SnS QDs. The optical characteristics of SnS QDs synthesized at pH 3 using various thiol capping agents are shown in Fig. 3.

Fig. 3(a) overlays the relevant UV–vis spectra of the thiol-capping QDs. Similar wide absorption bands centered at about 235 nm were present in the UV–vis absorption spectra of the various thiol-capped SnS QDs. The least absorbent QDs were L-cysteine-coated SnS QDs, whereas MPA and GSH exhibited comparable absorption spectra. Herein, the absorption and PL of QDs were affected by altering the capping thiols. Fig. 3(b–d) shows similar luminous characteristics observed in SnS QDs capped with MPA and L-cysteine, with MPA exhibiting the highest PL emission. This was explained by the possibility that MPA chelates Sn^{2+} more effectively than L-cysteine. L-cysteine is a bifunctional ligand with the amine and carboxyl groups as dragging bonds. As a result, the QDs surface experiences competitive coordination. Since MPA contains only carboxyl groups, it provides a better environment for coordinating the carboxylate anion with the tin metal. Han et al. [24], observed that MPA-functionalized SnS QDs were very stable even in cell culture because the MPA neutralized the surface charge. For GSH-capped SnS QDs (Fig. 3(d)), two emission peaks (at 360 nm and 650 nm) were observed. The peak at 650 nm was attributed to possible deep trap-state emissions, while the peak in the UV–vis region is characteristic of surface emissions [27,28].

5.5. The influence of ZnS passivation to form SnS/ZnS QDs

Since the bandgap of ZnS (3.6 eV) entirely covers that of SnS (1.5 eV), ZnS was selected as the shell material to (i) convert the QDs to type 1 core/shell structure and (ii) eliminate lattice mismatch [29,30]. The pH was regularly measured and kept at 3 for ideal reaction conditions throughout the shelling process. Fig. 4 depicts the optical characteristics of SnS QDs after ZnS passivation. Compared to SnS core QDs, the PL of SnS/ZnS QDs had a broad and red-shifted peak (from 350 nm to 500 nm). The peak shift and increase in intensity were attributed to ZnS passivating the surface of SnS QDs; these results align with the reported literature [19,28]. The matching UV–vis also showed a large shift towards longer wavelengths, indicating that the particle size of the QDs may have increased following ZnS coating. Therefore, passivating the MPA-capped SnS QDs with a ZnS shell improved the solubility and stability of the synthesized QDs in this study.

The TEM images of MPA-capped SnS QDs and SnS/ZnS QDs are shown in Fig. S1. Fig. S1(a) shows that the SnS QDs (2.20 nm) and SnS/ZnS QDs had tiny and nearly spherical particles; due to the tiny particle sizes and interparticle edges of the SnS/ZnS QDs, the TEM images could not be utilized to approximate the diameter and thickness of the shell (Fig. S1(b)). The SnS/ZnS QDs TEM monograph displayed particle lattice fridges at 20 nm magnification, indicating that nanocrystalline QDs were produced. The XRD diffraction peaks of the powered SnS/ZnS QDs are shown in Fig. 4(b). In line with the literature, the three peaks at $2\theta = 28.9°$, $48.6°$ and $56.1°$ correspond to (111), (220), and (311) planes associated with zinc blende structure were observed [24,30]. The widened XRD peaks confirm the TEM results, which indicate the small size of nanoparticles.

Elemental analysis of the synthesized SnS core and SnS/ZnS QDs was examined using Energy-dispersive X-ray spectroscopy (EDS), as shown in Fig. 5(a and b). The SnS QDs exhibited the expected Sn and S elements, while the presence of additional peaks of Zn and increased intensity of the S peak in the SnS/ZnS QDs was attributed to the ZnS shell layer. The capping agent accounted for the observed O and C peaks. The hydrodynamic (HD) size of SnS QDs and SnS/ZnS QDs was determined using dynamic light scattering (DLS). From Fig. 5(c) and (d), the SnS QDs exhibited a single narrow peak confirming excellent particle dispersion, while the passivated SnS/ZnS QDs exhibited two peaks suggesting a low concentration of smaller particles. The increase in size from the core

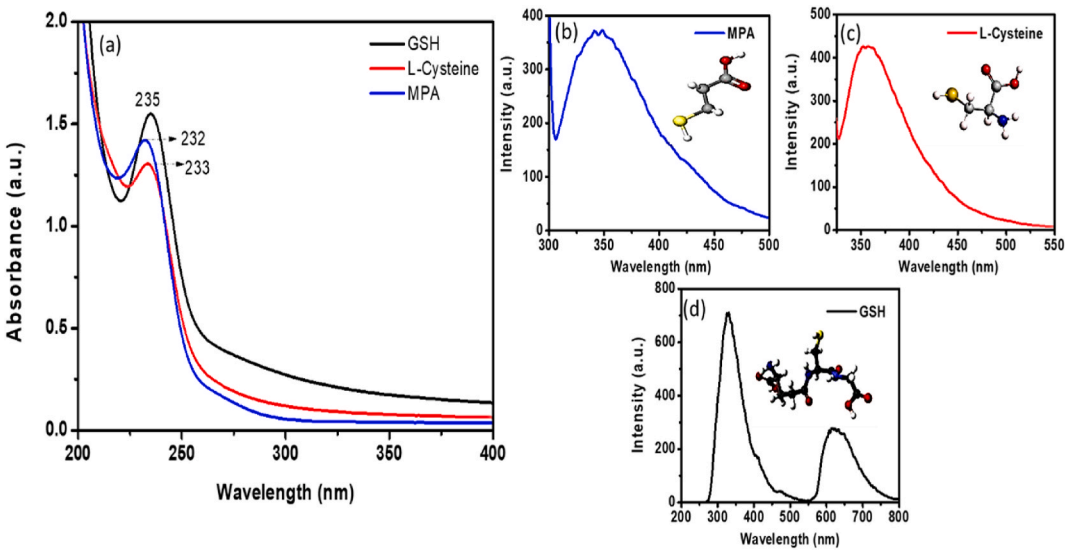

Fig. 3. Influence of thiol capping agents on (a) absorption spectra of SnS QDs coated with GSH, L-Cysteine and MPA. PL emissions of (b) GSH, (c) L-Cysteine and (d) MPA-capped SnS QDs.

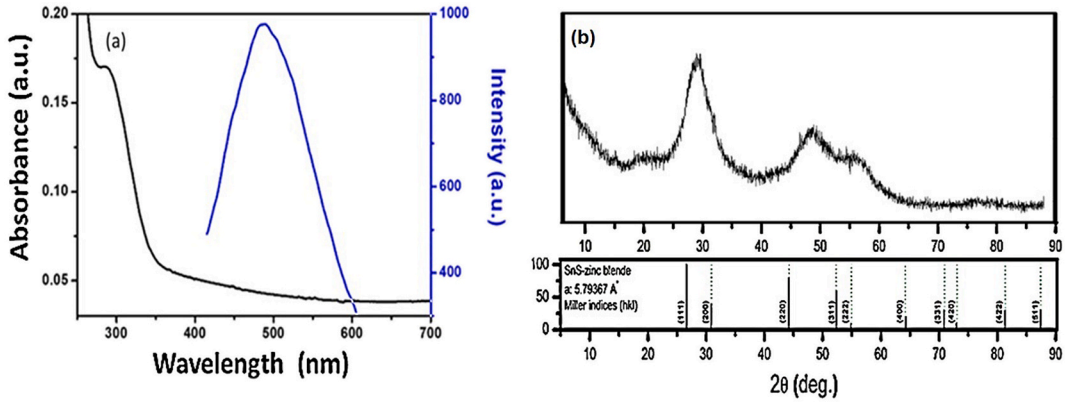

Fig. 4. (a) Overlay of photoluminescence and UV–vis spectra of SnS QDs passivated with ZnS shell. (b) XRD of SnS/ZnS QDs.

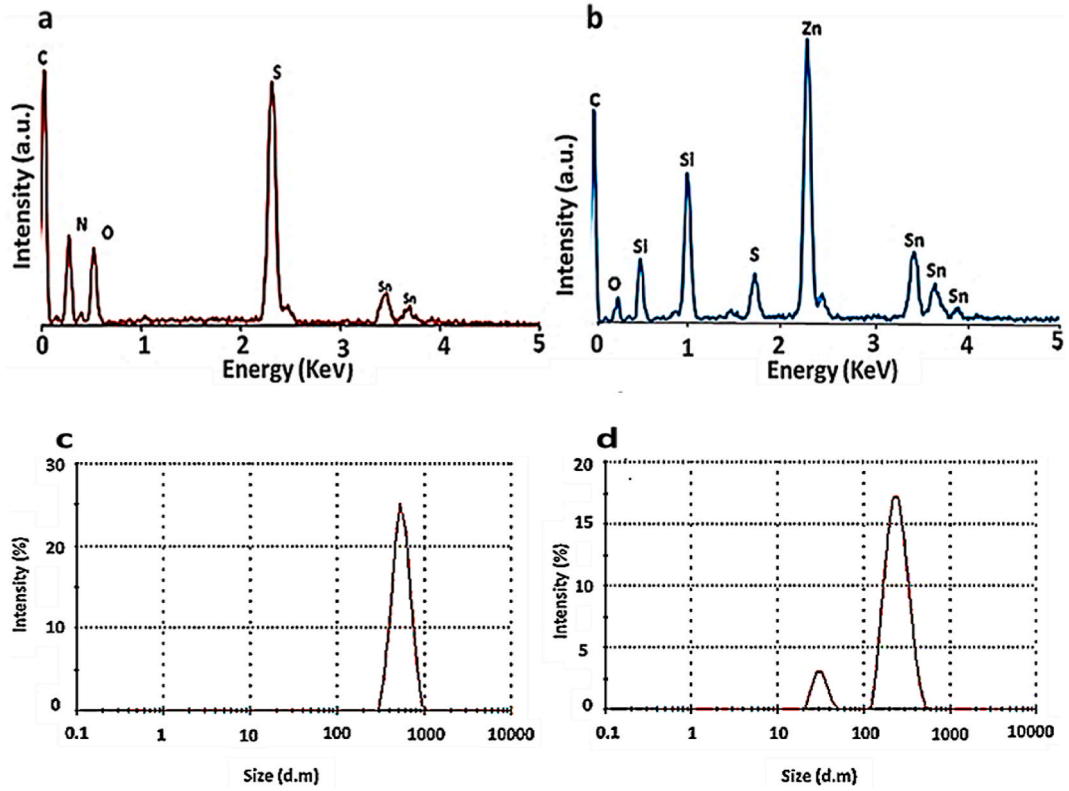

Fig. 5. EDS spectra of a) SnS QDs and b) SnS/ZnS QDs. DLS size distribution of (c) SnS QDs and (d) SnS/ZnS QDs.

QDs to ZnS-coated SnS QDs further confirms the surface coating of the core SnS QDs by a ZnS shell. SEM micrographs of the QDs taken before and after shell passivation are shown in Fig. S2. A change in surface morphology was observed after ZnS coating with the SnS core QDs exhibiting a flaky layered surface, while the SnS/ZnS QDs showed a crush-like morphology and rough surface.

5.6. Fourier transform infrared (FT-IR) spectroscopy analysis

FTIR analysis of the capped QDs was evaluated to determine the surface functional groups on the QDs. Fig. 6 shows the FTIR spectra of the combined GSH, L-Cysteine, and MPA-capped QDs. The typical hydroxyl (-OH) stretching vibrations of GSH-SnS/ZnS QDs were seen at 3306 cm^{-1} [31], and the asymmetrical and symmetrical stretching of the -N-H were observed at 2970 cm^{-1} and 2959 cm^{-1}, respectively (Fig. 6). While the peak at 1376 cm^{-1} was attributed to symmetric –COO, the bands at 1643 cm^{-1} were allocated to –C═O stretching. The absence of a thiol band (-SH, 2518 cm^{-1}) in GSH-SnS/ZnS QDs, confirms the GSH surface capping on the QDs. The

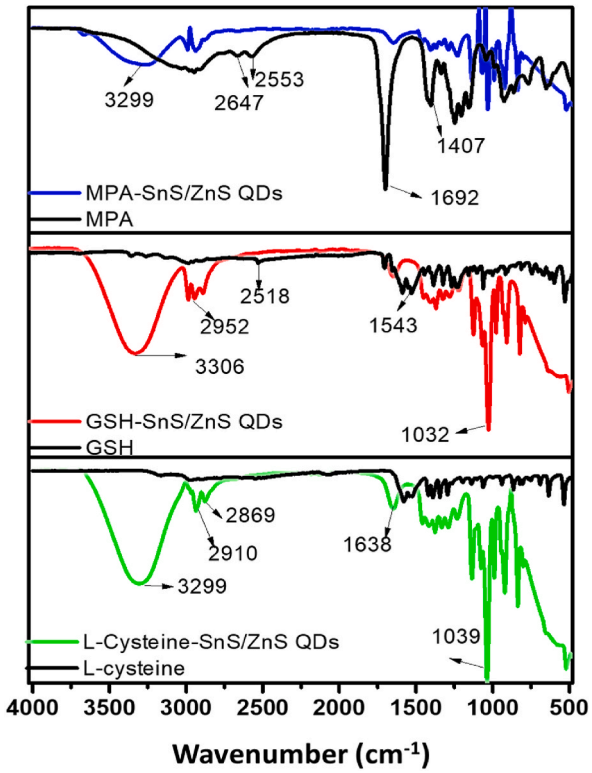

Fig. 6. FTIR analysis of MPA, GSH, and L-Cysteine capped SnS/ZnS QDs.

L-cysteine-capped SnS/ZnS QDs exhibited anti-symmetrical and asymmetrical stretching vibrations of $–CH_2$ were detected in the FT-IR spectra at 3299 cm^{-1}, 2910 cm^{-1}, and 2869 cm^{-1}, respectively, for the pure L-cysteine and Cys-SnS/ZnS QDs. The creation of the sharp band at 1039 cm^{-1} ($-NH_2$) structure in Cys-SnS/ZnS QDs, which is not present in pure L-Cysteine, and the shift at 1638 cm^{-1} (asymmetric stretching vibration of COO-) in these materials indicate –S═O stretching [31].

For MPA capping, the bands at 2989 cm^{-1} and 2932 cm^{-1} (red-shifted from pure MPA) were assigned to the asymmetric and symmetric –CH stretching, respectively. The peak at 3299 cm^{-1} was attributed to the O–H stretching of carboxylic acid [31]. After MPA capping, bands at 2674 cm^{-1} and 2553 cm^{-1} that were recognized as S–H stretching peaks from pure MPA power disappeared in the MPA-coated QDs; this explained the route of MPA passivation through thiol (-S-H) formed on the surface of the SnS/ZnS QDs, in-line with reported literature [32]. The considerable drop in –C═O (1692 cm^{-1}) band intensity and the other vibrational changes seen following MPA functionalization suggested that MPA was successfully capped on the surface of SnS/ZnS QDs. The thiols may have altered the surface of the QDs, as shown by the FTIR spectrum via the alterations in the thiol-capped QDs. It can be assumed that the QDs were successfully functionalized with thiols and thus possess bioactive terminal groups (viz amino and carboxylic groups), allowing further linking to biomolecules. As a result of the prolonged stability of MPA- SnS QDs, enhanced luminescence, and FTIR, MPA was selected as a capping agent in this study.

5.7. *The mechanism for the formation of SnS and SnS/ZnS QDs*

This study used propylene glycol (PG) as a complexing agent and solvent. Because of the two hydroxyl groups on PG, it can form complexes with other metal ions. It is thought that PG forms a complex with Sn^{2+}. When thiourea solution is introduced to the Sn^{2+}- PG reaction mixture, a competitive reaction for Sn^{2+} occurs. The Sn^{2+}-PG complex thermally decomposes with continuous heating, resulting in the rupture of coordinate bonds between Sn^{2+} and PG and the release of the Sn^{2+} into the solution. The hydroxyl groups on PG are crucial for size control and prevent many free Sn^{2-} from being produced in the solution. The formation of the Sn-thiourea complex [Sn (SCN_2H_4) n]$^{2+}$ causes a change in the color of the solution. The pH of the solution was adjusted and kept at pH 3 to ensure the stability of SnS QDs and to dissolve the strong coordinated bond of the Sn-thiourea complex. The MPA capping agent neutralizes the surface charge of the [Sn (SCN_2H_4) n]$^{2+}$ complex, stabilizing the SnS QDs. At the same time, the ZnS passivates the core surface, increasing the optical and quality of the synthesized QDs [24,26,30,31,33].

5.8. *Evaluation of the photocatalytic activity of the synthesized SnS QDs*

Prior to the photocatalytic analysis, spectroscopic studies of the dye and QDs alone were conducted to ensure potential

compatibility for energy transfer. The UV–vis spectra of the Rhodamine 6G (R6G) dye alone after light exposure revealed a prominent absorption band at 527 nm (with no secondary peak) with negligible variations in dye absorption (Fig. 7(a)). The dye colour (inset Fig. 7(a)) remained constant during the radiation, suggesting that the dye does not self-decompose [34]. Fig. 7(b) and (c) depict changes in the UV–vis absorption spectra of R6G dye in the presence of the SnS QDs and SnS/ZnS QDs, respectively, as a catalyst after 120 min of UV–vis light irradiation. The UV–vis peak position remained constant during the dye degradation process, with no new peak formation, suggesting that the degradation process did not aggregate the QDs or produce undesirable interferences [35].In addition, the overlap of the SnS/ZnS QDs emission spectra with the absorption of the dye suggests potential energy transfer compatibility and, therefore, possible dye photocatalytic degradation. Upon light illumination, in the presence of SnS core QDs, 31 % of the dye photodegraded within 120 min (Fig. 7(b)).

Notably, QDs passivated with ZnS degraded more quickly. The QDs passivated with ZnS demonstrated up to 65 % degrading efficiency with considerable dye solution decolourization (inset Fig. 7(c)). The addition of SnS/ZnS QDs increased the degradation efficiency because the ZnS shell promotes the separation of the photogenerated electron-hole pair, minimizing recombination [36]. Furthermore, the ZnS shell has a greater band gap (2.41 eV) than the SnS shell (1.3 eV), restricting light absorption, resulting in lower absorbance of the QDs, thus enhancing degrading characteristics of the core-shell QDs [37]. Additionally, the enhanced photodegradation might be due to the uniform deposition of SnS QDs onto the ZnS shell's surface, facilitating a more accessible charge transport mechanism for proceeding with the photocatalysis reaction. Moreover, the negatively charged nature of SnS-based QDs has been reported to be responsible for their superior photocatalytic performance against cationic dyes [38].

The degradation efficiency of SnS/ZnS QDs of 65 % is comparable to the values published for other nanomaterials as photocatalysts (Table S3 and Fig. S4). The results of this study reveal the SnS QDs and SnS/ZnS QDs exhibit promising photocatalytic properties, and the efficiency is further enhanced when the QDs are coated with ZnS. This application has direct implications for the remediation of environmental pollutants.

Based on the observations and discussions outlined above, the enhanced performance of SnS/ZnS QDs in the decomposition of the R6G dye could be caused by the positive synergistic interaction between SnS core and ZnS shell. Firstly, the cationic R6G molecules are easily attached to the surface of SnS nanoparticles by three approaches: electrostatic attraction, the π-π conjugation of the negatively charged structure, part π-conjugation system, and the great specific area. This adsorption improvement increases the effective concentration of R6G dye molecules near the surfaces of the core-shell SnS/ZnS QDs, resulting in a high catalytic degradation rate. Then, the wettability of the photocatalyst in an aqueous solution was enhanced by the hydrophilic groups, which are the results of the thiol capping on the surface of the core, which led to the good dispersion of SnS/ZnS QDs in the liquid phase. Furthermore, good contact between SnS and ZnS shell prevented the SnS core from leaking out during the catalytic processes, which effectively produced free •OH radicals species and ultimately aided in the degradation of R6G molecules, hence the appreciable improvement in the decomposition of the dye compared to the bare SnS QDs [34]. Although the photocatalytic process reported in this exhibited an effective degradation of R6G, it is worth noting that its applicability was only evaluated under UV light irradiation. At the same time, wastewater treatment requires visible-light-driven photocatalysts capable of absorbing throughout the solar spectrum [38]. Therefore, further studies are recommended to evaluate the SnS QDs' applicability in the visible region to enhance its applicability.

The mechanism for photodegradation of Rhodamine 6G (R6G)

As per Scheme 1, we propose the following mechanism and equation for dye degradation using SnS -based QDs as catalysts. Firstly, when the synthesized QDs were irradiated with UV light, an electron was transferred from the valency to the conduction band. This results in a high number of electron (e^-) and hole (h^+) pairs being formed (Eq. (1).).

$$SnS + h\nu \rightarrow SnS\ (e^-_{cb} + h^+_{vb})\ (1)$$

$$h^+_{vb} + H_2O \rightarrow H^+ + \bullet OH \quad (2)$$

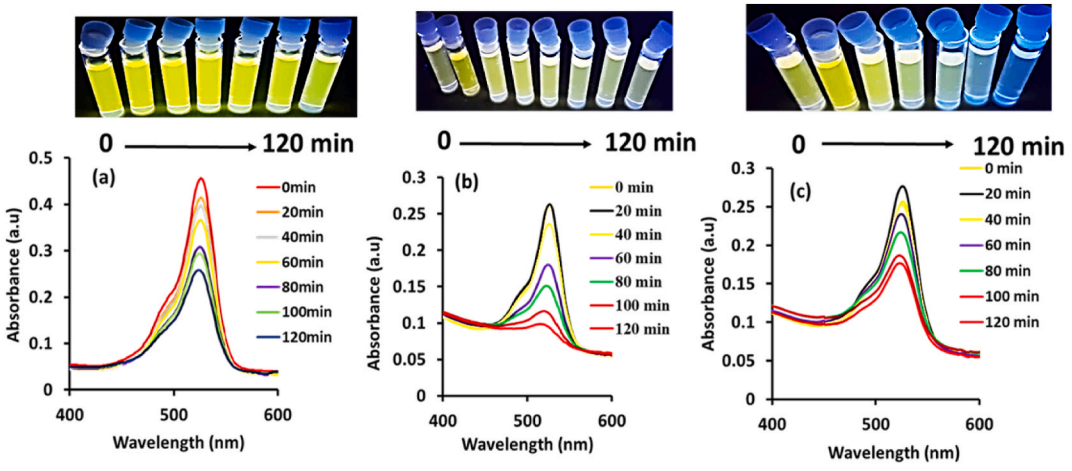

Fig. 7. Absorption spectra of R6G: (a) alone, (b) + SnS QDs, and (c) + SnS/ZnS core-shell QDS.

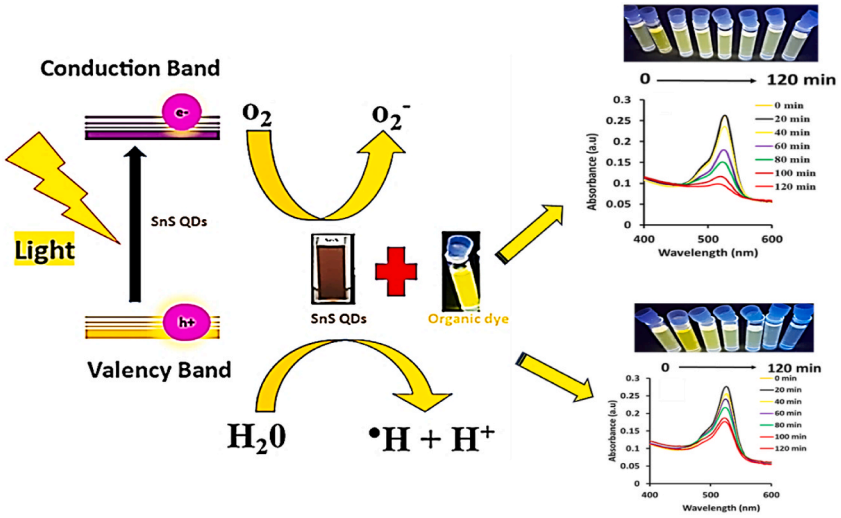

Scheme 1. Schematic presentation of possible photodegradation of the Rhodamine R6G dye.

$$h_{vb}^{+} + OH^{-} \rightarrow \bullet OH \quad (3)$$

$$\bullet OH + \text{dye} \rightarrow \text{degradation of dye} \quad (4)$$

The generated e^- subsequently reacted with O_2, forming reactive oxygen species (ROS) (i.e., H_2O_2, O^-, O_2^-), while the generated h^+ reacted with OH^- (derived from H_20) to form hydroxyl radicals (Equations (2) and (3)). The R6G dye molecules are then photodegraded by the oxygen-forming ROS and hydroxyl radicals (CO_2, H_2O and other mineralization) products (Eq. (4).) [38]. Here, the synthesis of QDs in propylene glycol further benefits the degradation process. The synthesized QDs can catalyze PG to decompose into more OH • radicals, further triggering the production of other radicals that can fully oxidize the R6G dye [39]. Moreover, R6G is a cationic dye that can dissociate into positively charged ions [37], aiding a strong interaction with negatively charged SnS QDs.

6. Conclusion

Herein we reported on a straightforward one-pot technique to synthesize thiolated SnS QDs using propylene glycol as a reaction solvent and complexing agent. The SnS-based QDs were produced under various experimental conditions, with the Sn: S ratio tuned to 1: 1 and the pH set to 3. Compared to GSH and L-Cysteine-capped SnS/ZnS QDs, MPA-capped QDs displayed greater stability. The QDs' luminescence intensities and absorption characteristics were enhanced after ZnS passivation. TEM revealed tiny, spherical, and evenly dispersed particles of SnS QDs and SnS/ZnS QDs. XRD patterns verified the zin blend morphology of the SnS/ZnS QDs. The photocatalytic activity of the QDs against R6G revealed that the dye was decoloured entirely in the presence of the QDs. The study also showed that dye degradation was accelerated in the presence of a ZnS shell compared to core SnS QDs. These findings suggest that SnS-based QDs passivated with ZnS as suitable for photocatalytic dye degradation.

Ethics declarations

Informed consent was not required for this study because the study did not involve animals, live vertebrates, and higher invertebrates.

Data availability

Data will be made available on request.

CRediT authorship contribution statement

Madillo Mareka: Writing – original draft, Methodology, Investigation, Formal analysis. **Mangaka Matoetoe:** Writing – review & editing, Supervision, Resources, Data curation. **Ncediwe Tsolekile:** Writing – review & editing, Writing – original draft, Supervision, Project administration, Funding acquisition, Conceptualization.

Declaration of competing interest

The authors declare that they have no known competing financial interests or personal relationships that could have appeared to influence the work reported in this paper.

Acknowledgments

The authors thank the National Research Foundation (NRF), South Africa, under the Thuthuka Grant (Grant No:121986), Cape Peninsula University of Technology, Chemistry Department, South Africa.

Appendix A. Supplementary data

Supplementary data to this article can be found online at https://doi.org/10.1016/j.heliyon.2024.e24191.

References

[1] B. Azanaw, B. Birlie, M. Teshome, Jemberie, Textile effluent treatment methods and eco-friendly resolution of textile wastewater, Case Stud. Chemic. Environ. Engin 6 (2022) 100230.
[2] S. Ledakowicz, K. Pa′zdzior, Recent achievements in dyes RemovalFocusedonAdvanced OxidationProcessesIntegratedwith BiologicalMethods, Molecules 4 (2021) 870–915.
[3] N. Qutub, P. Singh, S. Sabir, S. Sagadevan, O. Won-Chun, Enhanced photocatalytic degradation of Acid Blue dye using CdS/TiO_2 nanocomposite, Sci. Rep. 12 (2022) 5759.
[4] M. Thanavel, S.K. Kadam, S. P Biradar, S.P. Govindwar, B.-H. Jeon, S.K. Sadasivam, Combined biological and advanced oxidation process for decolorization of textile dyes, SN Appl. Sci. 1 (2019) 97.
[5] T. Borjigin, M. Schmitt, F. Morlet-Savary, P. Xiao, J. Lalevée, Low-cost and recyclable photocatalysts: metal oxide/polymer composites applied in the catalytic breakdown of dyes, Photochem 2 (2022) 733–751.
[6] M.A. Al-Nuaim, A.A. Alwasiti, Z.Y. Shnain, The photocatalytic process in the treatment of polluted water, Chem. Pap. 77 (2023) 677–701.
[7] N.K. Gupta, Y. Ghaffari, S. Kim, Photocatalytic degradation of organic pollutants over MFe_2O_4 (M = Co, Ni, Cu, Zn) nanoparticles at neutral pH, Sci. Rep. 10 (2020) 4942.
[8] G. Tripti, R.P. Chauhan, Adsorptive and photocatalytic properties of metal oxides towards arsenic remediation from water: a review, J. Environ. Chem. Eng.V. 9 (2021) 106734.
[9] P. Raizada, V. Soni, A. Kumar, P. Singh, A.A.P. Khan, A.M. Asiri, V.K. Thakur, V. Nguyen, Surface defect engineering of metal oxides photocatalyst for energy application and water treatment, J. Materiomics. 7 (2021) 388, 48.
[10] X. Guo, F. Zhang, Y. Zhang, J. Hu, Review on the advancement of SnS_2 in photocatalysis, J. Mater. Chem. A 11 (2023) 7331–7343.
[11] M. Cheraghizade, F. Jamali-Sheini, R. Yousefi, F. Niknia, M.R. Mahmoudian, M. Sookhakia, The effect of tin sulfide quantum dots size on photocatalytic and photovoltaic performance, Mater. Chem. Phys. 195 (2017) 187–194.
[12] Y. Lei, J. Zhou, Y. Chai, Y. Zhou, R. Yuan, Y. Lei, J. Zhou, Y. Chai, Y. Zhou, R. Yuan, SnS_2 quantum dots as new emitters with strong electrochemiluminescence for ultrasensitive antibody detection, Analyt. Chem. 90 (2018) 12270–12277.
[13] E. Daz-Cruz, E. Regalado-Pérez, J. Santos, H. Hu, Development of SnS/PVP core/shell quantum dots with tunable color emission synthesized by microwave heating, J. Solid State Chem. 300 (2020) 122264.
[14] A. Chowdhury, B. Shambharkar, S. Ghugal, S. Umare, S.A. Shende, Ethylene glycol mediated synthesis of SnS quantum dots and their application towards degradation of eosin yellow and brilliant green dyes under solar irradiation, RSC Adv. 6 (2016) 108290–108297.
[15] M. Miyauchi, Y. Shiga, N. Srinivasan, D. Atarashi, E. Sakai, Ubiquitous quantum dot-sensitized nanoporous film for hydrogen, Mater. Chem. Phys. 160 (2015) 383–388.
[16] R. Srivastav, V.K. Signh, A. Srivastav, pH dependent luminescence switching of tin disulfide quantum dots, J. Lumin. 213 (2019) 401–408A.
[17] M. Upadhyay, A. Thakur, Synthesis and characterization of tin sulfide nanoparticles M, Sci. Amp; Tech. J 7 (2019) 102–104.
[18] J. Jacob, R. Rajan, M. Aji, G. Kurup, A. Pugazhendhi, Bio-inspired ZnS quantum dots as efficient photo catalysts for the degradation of methylene blue in aqueous phase, Cer. Inter. 45 (2019) 4857–4862.
[19] O. Cheng, Acar, Y. Shih, H. Shih, pH dependent luminescence switching of tin disulfide quantum dots, Chem. Phys. Letters 754 (2020) 137696.
[20] R. Ayranci, M. Ak, Synthesis of a novel, fluorescent, electroactive and metal ion sensitive thienylpyrrole derivate, New J. Chem. 40 (2016) 8053.
[21] S. P arani, N. Tsolekile, K. Pandian, O.S. Oluwafemi, Thiolated selenium as a new precursor for the aqueous synthesis of CdSe/CdS core/shell quantum dots, J. Mater. Sci. Mater. Electron. 28 (2017) 11151–11162.
[22] H.Y. Cheng, O. Acar, W.Y. Shih, W.-H. Shih, Enhancing the photoluminescence of SnS quantum dots by ZnS treatment, Chem. Phys. Lett. 754 (2020) 137696.
[23] R. Miranti, R. Septianto, T. Kikitsu, D. Hashizume, N. Matsushita, Y. Iwasa, S. Bisri, π-SnS colloidal nanocrystals with size-dependent band gaps, J. Phys. Chem. C 126 (2022) 5323–5332.
[24] S. Han, W. Shih, W. Shih, Charge-neutral, stable, non-cytotoxic, near-infrared SnS aqueous quantum dots for high signal-to-noise-ratio biomedical imaging, Chem. Select. 2 (2017) 7332–7339.
[25] R. Ayranci, M. Ak, Synthesis of a novel, fluorescent, electroactive and metal ion sensitive thienylpyrrole derivate, New J. Chem. 40 (2016) 8053.
[26] T. D Nguyen, T. O Do, Size- and Shape-Controlled Synthesis of Monodisperse Metal Oxide and Mixed Oxide Nanocrystals, Nanocrystal. InTech, 2011.
[27] Y. Kim, J. Chang, H. Choi, Y. Kim, W. Bae, S. Jeong, III–V colloidal nanocrystals: control of covalent surfaces, Chemical Science, Chem. Sci. 11 (2020) 913–922.
[28] A. Chowdhury, B. Shambharkar, S. Ghugal, S. Umare, S.A. Shende, Ethylene glycol mediated synthesis of SnS quantum dots and their application towards degradation of eosin yellow and brilliant green dyes under solar irradiation, RSC Adv. 6 (2016) 108290–108297.
[29] C. Park, Y.S. Nam, Controlling surface defects of non-stoichiometric copper-indium-sulfide quantum dots, J. Colloid Interface Sci. 460 (2015) 173–180.
[30] M. Miyauchi, Y. Shiga, N. Srinivasan, D. Atarashi, E. Sakai, Ubiquitous quantum dot-sensitized nanoporous film for hydrogen, Mater. Chem. Phys. 160 (2015) 383–388.
[31] G. Veerasubramani, M. Park, J. Choi, D. Kim, Ultrasmall SnS quantum dots anchored onto nitrogen-enriched carbon nanospheres as an advanced anode material for sodium-ion batteries, Appl. Mater. & Amp; Interf. 12 (2020) 7114–7124.
[32] J. Jacob, R. Rajan, M. Aji, G. Kurup, A. Pugazhendhi, Bio-inspired ZnS quantum dots as efficient photo catalysts for the degradation of methylene blue in aqueous phase, Cer. Inter. 45 (2019) 4857–4862.
[33] M. Upadhyay, A. Thakur, Synthesis and characterization of tin sulfide nanoparticles M, Sci. Amp; Tech. J 7 (2019) 102–104.
[34] I. Groeneveld, M. Kanelli, F. Ariese, Parameters that affect the photodegradation of dyes and pigments in solution and on substrate – an overview, Dyes Pigments 210 (2013) 110999.

[35] M. Rochkind, S. Pasternak, Y. Paz, Using dyes for evaluating photocatalytic properties: a critical review, Molecules 20 (2015) 88–110.
[36] D. Prabha, K. Usharani, S. Ilangovan, V. Narasimman, S. Balamurugan, M. Suganya, J. Srivind, V.S. Nagarethinam, A.R. Balu, Thermal behavior and comparative study on the visible light driven photocatalytic performance of SnS_2–ZnS nanocomposite against the degradation of anionic and cationic dyes, J. Mat. Sci. Mat. in Electr 29 (2018) 18708–18717.
[37] N. Thirugnanam, H. Song, Y. Wu, Photocatalytic degradation of Brilliant Green dye using CdSe quantum dots hybridized with graphene oxide under sunlight irradiation, Chin. J. Catal. 38 (2017) 2150–2159.
[38] V. Lp, V. Rajagopalan, A new synergetic nanocomposite for dye degradation in dark and light, Sci. Rep. 6 (2016) 38606.
[39] Y.-H. Chiu, T.-F.M. Chang, C.-Y. Chen, M. Sone, Y.-J. Hsu, Mechanistic insights into photodegradation of organic dyes using heterostructure photocatalysts, Catalysts 9 (2019) 430.